



8 **Abstract**

9 Transcripts are frequently modified by structural variations, which leads to either a fused transcript of  
10 two genes (known as a fusion gene) or an insertion of intergenic sequence into a transcript. These mod-  
11 ifications, called transcriptomic structural variants (TSV), can lead to drastic changes in a downstream  
12 product. Detecting TSVs, especially in cancer tumor sequencing where they are known to frequently  
13 occur, is an important and challenging computational problem. This problem is made even more chal-  
14 lenging in that often only RNA-seq measurements are available. We introduce SQUID, a novel algorithm  
15 and its implementation, to accurately predict both fusion-gene and non-fusion-gene TSVs from RNA-  
16 seq alignments. SQUID takes the unique approach of attempting to reconstruct an underlying genome  
17 sequence that best explains the observed RNA-seq reads. By unifying both concordant alignments and  
18 discordant read alignments into one model, SQUID achieves high sensitivity with many fewer false pos-  
19 itives than other approaches. We detect TSVs on TCGA tumor samples using SQUID, and observe that  
20 that non-fusion-gene TSVs are more likely to be intra-chromosomal than fusion-gene TSVs. We also  
21 quantify the propensity for breakpoint partners to be reused. We identify several novel TSVs involving  
22 tumor suppressor genes, which may lead to loss-of-function in the corresponding genes and play a role  
23 in tumorigenesis.

24 **1 Introduction**

25 Large-scale transcriptome sequence changes are known to be associated with cancer (Mertens et al. 2015,  
26 Sveen et al. 2015). Those changes are usually a consequence of genomic structural variation (SV). By  
27 pulling different genomic regions together or separating one region into pieces, structural variants can po-  
28 tentially cause severe alteration to transcribed or translated products. Transcriptome changes induced by  
29 genomic SVs, called transcriptomic structural variants (TSVs), can have a particularly large impact on dis-  
30 ease genesis and progression. In some cases, TSVs bring regions from one gene next to regions of another,  
31 causing exons from both genes to be transcribed into a single transcript (known as a fusion gene). Domains  
32 of the corresponding RNA or proteins can be fused, inducing new functions or causing loss of function, or  
33 the transcription or translation levels can be altered, leading to disease states. For example, *BCR-ABL1* is a  
34 well-known fusion oncogene for chronic myeloid leukemia (Deininger et al. 2000), and the *TMPRSS2-ERG*  
35 fusion product leads to over-expression of *ERG* and helps triggers prostate cancer (Tomlins et al. 2005).  
36 These fusion events are used as biomarkers for early diagnosis or treatment targets (Wang et al. 2008). In

37 other cases, TSVs can affect genes by causing a previously non-transcribed region to be incorporated into a  
38 gene, causing disruption to the function of the altered gene. There are fewer studies on these TSVs between  
39 transcribed and non-transcribed regions, but their ability to alter downstream RNA and protein structure is  
40 likely to lead to similar results as fusion gene TSVs.

41 Genomic SVs are typically detected from whole-genome sequencing (WGS) data by identifying reads and  
42 read pairs that are incompatible with a reference genome [e.g., Chen et al., 2009, Hormozdiari et al., 2010,  
43 Layer et al., 2014, Quinlan et al., 2010, Rausch et al., 2012]. However, WGS data are not completely suitable  
44 to infer TSVs since they neither inform which region is transcribed nor reveal how the transcribed sequence  
45 will change if SVs alter a splicing site or the stop codon. In addition, WGS data is more scarce and more  
46 expensive to obtain than RNA-seq (Sboner et al. 2011) measurements, which target transcribed regions  
47 directly. RNA-seq is relatively inexpensive, high-throughput, and widely available in many existing and  
48 growing data repositories. For example, The Cancer Genome Atlas (TCGA, <https://cancergenome.nih.gov>)  
49 contains RNA-seq measurements from thousands of tumor sample across various cancer types, but 80% of  
50 tumor samples in TCGA have RNA-seq data but no WGS data (Supp. Figure S1). While methods exist to  
51 detect fusion genes from RNA-seq measurements [e.g., Davidson et al., 2015, Iyer et al., 2011, McPherson  
52 et al., 2011, Nicorici et al., 2014, Zhang et al., 2016], fusion genes are only a subset of TSVs, and existing  
53 fusion gene detection methods rely heavily on current gene annotations and are generally not able or at least  
54 not optimized to predict non-fusion-gene TSV events. This motivates the need for a method to detect all  
55 types of TSVs directly from RNA-seq data.

56 We present SQUID, the first computational tool that is designed to comprehensively predict TSVs from  
57 RNA-seq data. SQUID divides the reference genome into segments and builds a genome segment graph  
58 from both concordant and discordant RNA-seq read alignments. In this way, it can detect both fusion-gene  
59 events and TSVs incorporating previously non-transcribed regions into transcripts. Using an efficient, novel  
60 integer linear program (ILP), SQUID rearranges the segments of the reference genome so that as many  
61 read alignments as possible are concordant with the rearranged sequence. TSVs are represented by pairs  
62 of breakpoints realized by the rearrangement. Discordant reads that cannot be made concordant through  
63 the optimal rearrangement given by the ILP are discarded as false positive discordant reads, likely due to  
64 misalignments. By building a consistent model of the entire rearranged genome and maximizing the number  
65 of overall concordant read alignments, SQUID drastically reduces the number of spurious TSVs reported

66 compared with other methods.

67 SQUID features high accuracy. SQUID is usually  $> 20\%$  more accurate than applying WGS-based SV  
68 detection methods to RNA-seq data directly. It is similarly more accurate than a pipeline that uses de novo  
69 transcript assembly and transcript-to-genome alignment to detect TSVs. We also show that SQUID is able  
70 to detect more TSVs involving non-transcribed regions than any existing fusion gene detection method.

71 We use SQUID to detect TSVs within 401 TCGA tumor samples of four cancer types (99–101 samples each  
72 of breast invasive carcinoma (Network et al. 2012), bladder urothelial carcinoma (Network et al. 2014a),  
73 lung adenocarcinoma (Network et al. 2014b), and prostate adenocarcinoma (Network et al. 2015)). SQUID's  
74 predictions suggest that breast invasive carcinoma has more samples with a larger or smaller number of  
75 TSVs / non-fusion-gene TSVs than other cancer types. We also characterize the differences between fusion-  
76 gene TSVs and non-fusion-gene TSVs. Non-fusion-gene TSVs, for example, are more likely to be intra-  
77 chromosomal events. We show that breakpoints can occur in multiple samples, and among those that do  
78 repeatedly occur, their breakpoint partners are also often conserved. Finally, we identify several novel  
79 non-fusion-gene TSVs that affect known tumor suppressor genes, which may result in loss-of-function of  
80 corresponding proteins and play a role in tumor genesis.

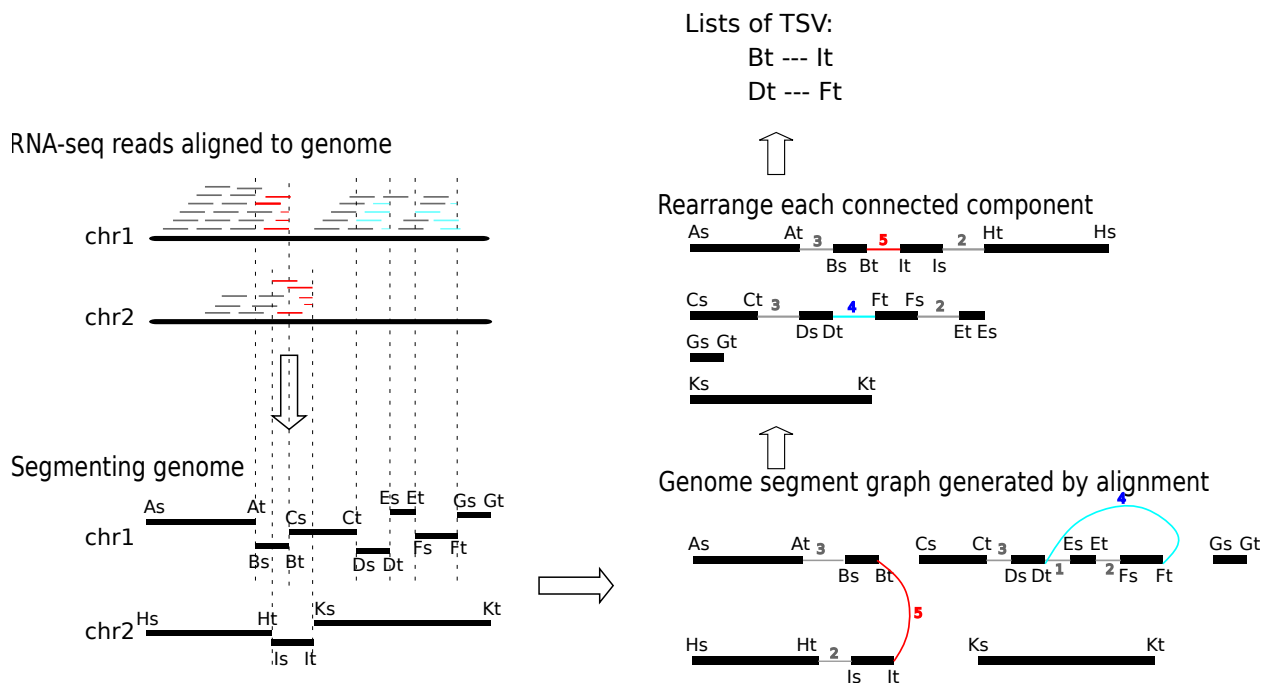
## 81 **2 Results**

### 82 **2.1 A novel algorithm for detecting TSVs from RNA-seq**

83 SQUID predicts TSVs from RNA-seq alignments to the genome (Figure 1 provides an overview). To do this,  
84 it seeks to rearrange the reference genome to make as many of the observed alignments consistent with the  
85 rearranged genome as possible. Formally, SQUID constructs a graph from the alignments where the nodes  
86 represent boundaries of genome segments and the edges represent adjacencies implied by the alignments.  
87 These edges represent both concordant and discordant alignments, where concordant alignments are those  
88 consistent with the reference genome and discordant alignments are those that are not. SQUID then uses  
89 a novel integer linear program (Section 4.2) to order and orient the vertices of the graph to make as many  
90 edges consistent as possible. Adjacencies that are present in this rearranged genome but not present in  
91 the original reference are proposed as predicted TSVs. The identification of concordant and discordant

alignments (Section 4.3), construction of the genome segments (Section 4.4), creation of the graph, and the reordering objective function (Section 4.1) are described in the Methods section.

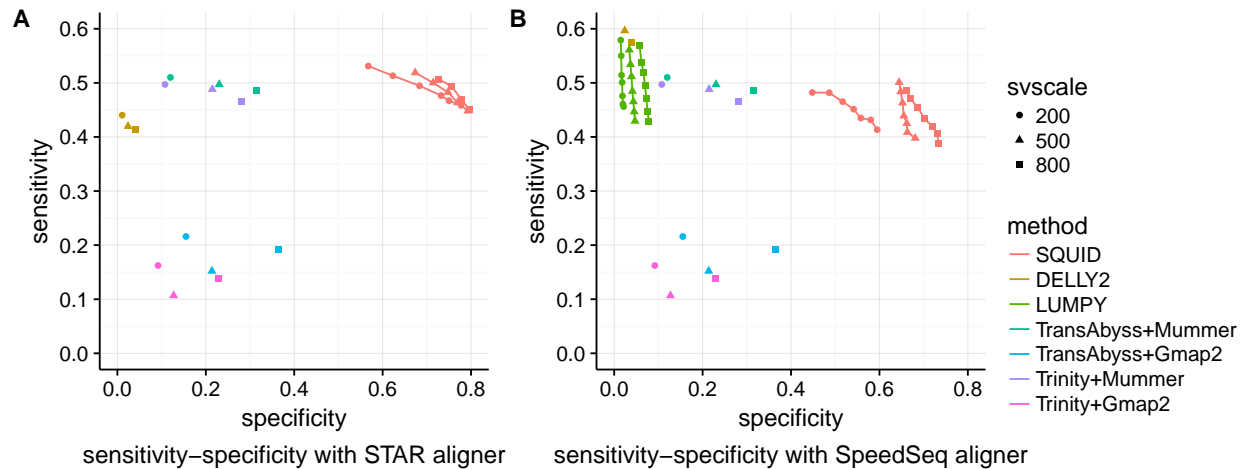
Figure 1: Overview of the SQUID algorithm. Based on the alignments of RNA-seq reads to the reference genome, SQUID partitions the genome into segments, connects the endpoints of the segments to indicate the actual adjacency in transcript, and finally reorders the endpoints along the most reliable path. Each edge in the final path that comes from discordant read alignments represents a TSV.



## 94 2.2 SQUID is accurate on simulation data

95 Overall, SQUID's predictions of TSVs are far more precise than other approaches at similar sensitivity  
96 on simulated data (Section 4.7). SQUID achieves 60% to 80% percent precision and about 50% percent  
97 sensitivity on simulation data (Figure 2). SQUID's precision is  $\approx 40\%$  higher than all combinations of  
98 de novo transcriptome assembly and transcript-to-genome alignment pipeline, and the precision of WGS-  
99 based SV detection methods on RNA-seq data is even lower. The sensitivity of SQUID is similar to de novo  
100 assembly with MUMmer3, but a little lower than DELLY2 and LUMPY with SpeedSeq aligner. The overall  
101 sensitivity is not as high as precision, which is probably because there are not enough supporting reads  
102 aligned correctly to some TSV breakpoints. The fact that assembly and WGS-based SV detection methods  
103 achieve similar sensitivity corroborates the hypothesis that it is the data limiting the achievable sensitivity.

Figure 2: Performance of SQUID and other methods on simulation data. Different number of SVs (200, 500, 800 SVs) are simulated in each dataset. Each simulated read is aligned with both (A) STAR and (B) SpeedSeq aligner. If the method allows for user-defined minimum read support for prediction, we vary the threshold from 3 to 9, and plot a curve on sensitivity-specificity curve (SQUID and LUMPY), otherwise it is shown as a single point



104 The low specificity of the pipeline- and WGS-based methods shows neither of these types of approaches  
105 are suitable for TSV detection from RNA-seq data. WGS-based SV detection methods are able to detect  
106 TSV signals, but not able to filter out false positives. Assembly-based approaches require solving the tran-  
107 scriptome assembly problem which is a harder and more time-consuming problem, and thus errors are more  
108 easily introduced. Further, the performance of assembly pipelines depends heavily on the choice of software  
109 — for example, MUMmer3 is better at discordantly aligning transcripts than GMAP.

110 SQUID's effectiveness is likely due to its unified model of both concordant reads and discordant reads.  
111 Coverage in RNA-seq alignment is proportional to the expression level of the transcript, and using one  
112 read count threshold for TSV evidence is not appropriate. Instead, the ILP in SQUID sets concordant and  
113 discordant alignments into competition and selects the winner as the most reliable TSVs.

### 114 2.3 SQUID is able to detect non-fusion-gene TSV on two previously-studied cell lines

115 Fusion gene events are a strict subset of TSVs where the two breakpoints are each within a gene region and  
116 the fused sequence corresponds to the sense strand of both genes. Fusion genes thus exclude TSV events  
117 where a gene region is fused with a intergenic region or an anti-sense strand of another gene. Nevertheless,

118 fusion genes have been implicated (likely because of available methods to detect them) in playing a role in  
119 cancer.

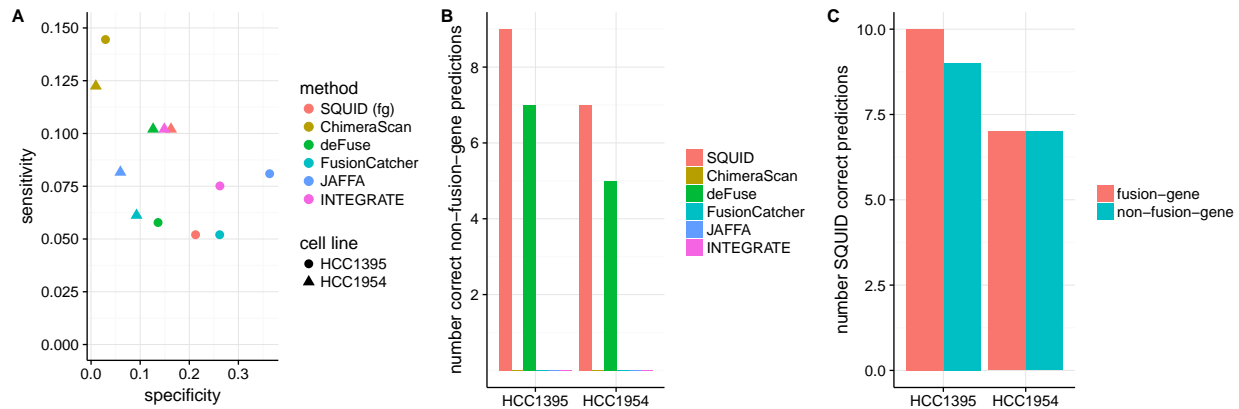
120 To probe SQUID's ability to detect this subclass of TSVs, we use two cell lines, HCC1954 and HCC1395,  
121 for which previous studies have experimentally validated predicted SVs and fusion gene events. Specifically,  
122 we compile results from Bignell et al. [2007], Galante et al. [2011], Stephens et al. [2009], Zhao et al. [2009]  
123 and Robinson et al. [2011] for HCC1954, and results from Stephens et al. [2009] and Zhang et al. [2016]  
124 for HCC1395. After removing short deletions and overlapping structural variations among different studies,  
125 we have 326 validated structural variations for HCC1954 cell line, in which 245 of them have at least one  
126 breakpoint outside a gene region, and the rest (81) have both breakpoints within gene region; we have 256  
127 validated true structural variations for HCC1395 cell line, in which 94 have at least one breakpoint outside  
128 a gene region, while the rest (162) have both breakpoints within gene. For a predicted structural variation to  
129 be true positive, both predicted breakpoints should be within a window of 30kb of true breakpoints and the  
130 predicted orientation should agree with the true orientation. We use a relatively large window since the true  
131 breakpoints can be located within an intron or other non-transcribed region, while the observed breakpoint  
132 from RNA-seq reads will be at a nearby coding or expressed region.

133 We use publicly available RNA-seq data from the NIH Sequencing Read Archive (SRA; accessions:  
134 SRR2532344 and SRR925710 for HCC1954, SRR2532336 for HCC1395). Because the data are from a  
135 pool of experiments, the sample from which RNA-seq was collected may be different from those used for  
136 experimental validation. We align reads to the reference genome using STAR.

137 When restricted to fusion gene events, SQUID achieves similar precision and sensitivity compared to fusion  
138 gene detection tools (Figure 3A). SQUID has the highest accuracy in HCC1954 cell line, with very similar  
139 sensitivity as all fusion gene detection tools. For HCC1395, SQUID is in the middle of fusion gene detection  
140 methods, while INTEGRATE and JAFFA are the best performers on this sample.

141 It is even harder to predict non-fusion-gene TSVs accurately, since current annotations cannot be used to  
142 limit the search space for potential read alignments or TSV events. Only SQUID and deFuse are able to  
143 detect non-fusion-gene events. Between these two methods, SQUID is able to predict more known non-  
144 fusion-gene TSVs correctly (Figure 3B). At the same time, the precision of SQUID does not decrease  
145 very much by considering both fusion-gene and non-fusion-gene TSVs (HCC1954: fusion gene specificity

Figure 3: Performance of SQUID and fusion gene detection methods on breast cancer cell lines HCC1954 and HCC1395. Predictions are evaluated by previously validated SVs and fusions. (A) Sensitivity-specificity of different methods for predicting fusion gene events on both cell lines. (B) Number of correct non-fusion-gene TSV predictions that correspond to previously validated SVs. (C) Number of correctly predicted fusion-gene TSVs and non-fusion-gene TSVs from SQUID. Non-fusion-gene TSVs makes up a considerable proportion of all TSVs.



146 is 16.28%, and overall specificity is 15.56%; HCC1395: fusion gene specificity is 21.28%, and overall  
147 specificity is 19.39%). A considerable proportion of validated TSVs are non-fusion-gene TSVs: correctly  
148 predicted non-fusion-gene TSVs compose almost half of all correct predictions of SQUID (Figure 3C).

#### 149 2.4 Charactering TSVs on four types of TCGA cancer samples

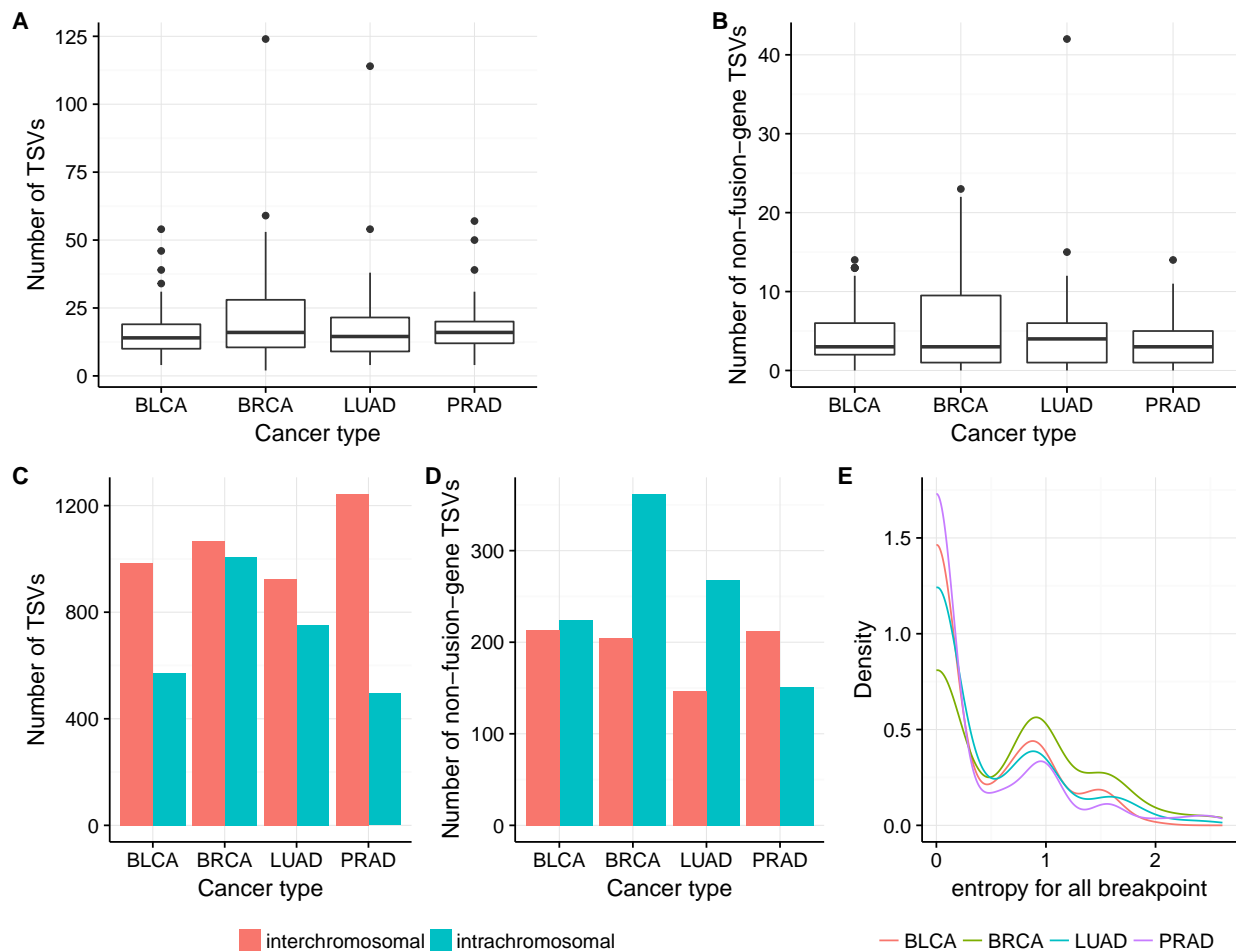
150 To compare the distributions and characteristics of TSVs among cancer types and between TSV types, we  
151 arbitrarily selected 99 to 101 tumor samples from TCGA for each of four cancer types: breast invasive  
152 carcinoma (BRCA), bladder urothelial carcinoma (BLCA), lung adenocarcinoma (LUAD), and prostate  
153 adenocarcinoma (PRAD).

154 To estimate the accuracy of SQUID's prediction on selected TCGA samples, we use WGS data of the  
155 same patients to validate TSV junctions. There are in total 72 WGS experiments available for the 400  
156 samples (20 BLCA, 10 BRCA, 31 LUAD, 11 PRAD). For each TSV prediction, we extract a 25Kb sequence  
157 around both breakpoints and concatenate them according to the predicted TSV orientation. We then map  
158 the WGS reads against these junction sequences using SpeedSeq. If a paired-end WGS read can only be  
159 mapped concordantly to a junction sequence but not the reference genome, that paired-end read is marked  
160 as supporting the TSV. If at least 3 WGS reads support a TSV, the TSV is considered as validated. Using

161 this approach, SQUID's overall validation rate is 88.21%, and this indicates that SQUID is quite accurate  
162 and reliable on TCGA data.

163 We find that most samples have  $\approx 15$ – $20$  TSVs including  $\approx 3$ – $5$  non-fusion-gene TSVs among all four  
164 cancer types (Figure 4A,B). BRCA has a longer tail on both sides of the distribution of TSV counts, where  
165 more samples contain a larger number of TSVs, and more samples contains a smaller number of TSVs. The  
166 same trend is observed when restricted to non-fusion-gene TSVs.

Figure 4: (A,B) Number of TSVs and non-fusion-gene TSVs in each sample in different cancer types. BRCA has slightly more samples with larger or smaller number of (non-fusion-gene) TSVs, thus showing a longer tail on both ends of y axis. (C,D) Number of inter-chromosomal and intra-chromosomal TSVs within all TSVs and within non-fusion-gene TSVs. Non-fusion-gene TSVs contain more intra-chromosomal events than fusion-gene TSVs. (E) For breakpoints occurring more than 3 times in the same cancer type, the distribution of the entropy of its TSV partner. The lower the entropy, the more likely the breakpoint has a fixed partner. The peak near 0 indicates a large portion of breakpoints are likely to be rejoined with the same partner in TSV. However, there are still some breakpoints that have multiple rejoined partners.



167 Inter-chromosomal TSVs are more prevalent than intra-chromosomal TSVs for all cancer types (Figure 4C),  
168 although this difference is much more pronounced in bladder and prostate cancer. Non-fusion-gene TSVs  
169 are more likely to have intra-chromosomal events than fusion gene TSVs (Figure 4D), and in fact in  
170 bladder, breast, and lung cancer, we detect more intra-chromosomal non-fusion-gene TSVs than inter-  
171 chromosomal non-fusion-gene TSVs. Prostate cancer is an exception in that, for non-fusion-gene TSVs,  
172 inter-chromosomal events are observed more often than intra-chromosomal events. Nevertheless, it also  
173 holds true that non-fusion-gene TSVs are more likely to be intra-chromosomal than fusion-gene, because  
174 the percentage of intra-chromosomal TSVs within non-fusion-gene TSVs is higher than that within all TSVs.

175 For a large proportion of breakpoints occurring multiple times within a cancer type, their partner in the TSV  
176 is likely to be fixed and to reoccur every time that breakpoint is used. To quantify this, for each breakpoint  
177 that occurred  $\geq 3$  times, we compute the entropy of its partner promiscuity. Specifically, we derive a  
178 discrete, empirical probability distribution of partners for each breakpoint and compute the entropy of this  
179 distribution. This measure thus represents the uncertainty of the partner given one breakpoint, with higher  
180 entropy corresponding to a less conserved partnering pattern. In Figure 4E, we see that there there is a high  
181 peak near 0 for all cancer types, which indicates that for a large proportion of recurring breakpoints, we  
182 are certain about its rejoined partner once we know the breakpoint. However, there are also promiscuous  
183 breakpoints with entropy larger than 0.5.

## 184 **2.5 Tumor suppressor genes can undergo TSV and generate altered transcripts**

185 Tumor suppressor genes (TSG) protect cells from becoming cancer cells. Usually their functions involve  
186 inhibiting cell cycle, facilitating apoptosis, and so on (Sherr 2004). Mutations in TSGs may lead to loss  
187 of function of the corresponding proteins and benefit tumor growth. For example, homozygous loss-of-  
188 function mutation in p53 is found in about half of cancer samples across various cancer types (Hollstein  
189 et al. 1991). TSVs are likely to cause loss of function of TSGs as well. Indeed, we observe several TSGs  
190 that are affected by TSVs, both of the fusion-gene type and the non-fusion-gene type.

191 The *ZFHX3* gene encodes a transcription factor that transactivates cyclin-dependent kinase inhibitor 1A  
192 (aka *CDKN1A*), a cell cycle inhibitor (Maglott et al. 2011). We find that in one BLCA and one BRCA  
193 sample, there are TSVs affecting *ZFHX3*. These two TSVs events are different from each other in terms of  
194 the breakpoint partner outside of *ZFHX3*. In the BLCA tumor sample, a intergenic region is inserted after

195 the third exon of *ZFHX3* (Figure 5A). The fused transcript stops at the inserted region, causing the *ZFHX3*  
196 transcript to lose the rest of its exons. In the BRCA tumor sample, a region of the anti-sense strand of gene  
197 *MYLK3* is inserted after the third exon of *ZFHX3* gene (Figure 5B). Because codons and splicing sites are  
198 not preserved on the anti-sense strand, the transcribed insertion region does not correspond to known exons  
199 of *MYLK3* gene, but covers the range of first exon of *MYLK3* and extend to the first intron and 5' intergenic  
200 region. Transcription stops within inserted region, and causes the *ZFHX3* transcript to lose exons after exon  
201 3, which resembles the fusion with intergenic region in BLCA sample.

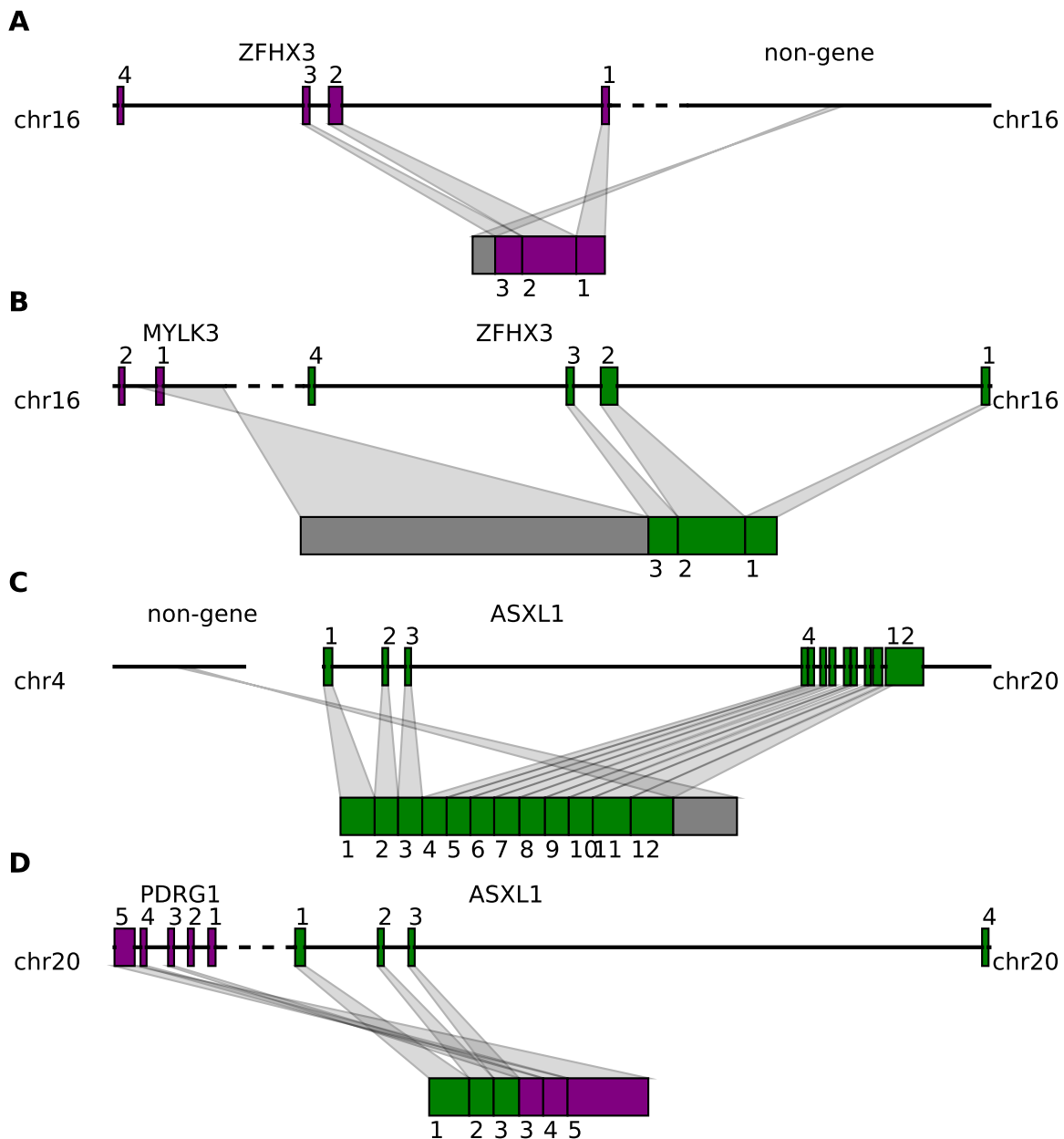
202 Another example is given by the *ASXLI* gene, which is essential for activating *CDKN2B* to inhibit tumorgen-  
203 esis (Wu et al. 2015). We observe two distinct TSVs related to *ASXLI* from BLCA and BRCA samples. The  
204 first TSV merges the first 11 exons and half of exon 12 of *ASXLI* with a intergenic region on chromosome 4  
205 (Figure 5C). Transcription stops at the inserted intergenic region, leaving the rest of exon 12 not transcribed.  
206 The breakpoint within the *ASXLI* is before the 3' UTR, so the downstream protein sequence from exon 12  
207 will be affected. The other TSV involving *ASXLI* is a typical fusion-gene TSV where the first three exons of  
208 *ASXLI* are fused with the last three exons from the *PDRGI* gene (Figure 5D). Protein domains after *ASXLI*  
209 exon 4 and before *PDRGI* exon 2 are lost in the fused transcript.

210 These non-fusion-gene examples are novel predicted TSV events that are not typically detectable via tradi-  
211 tional fusion-gene detection methods using RNA-seq data. They suggest that non-fusion-gene events can  
212 also be involved in tumorigenesis by causing disruption of tumor suppressor genes.

### 213 3 Discussion

214 We developed SQUID, the first algorithm for accurate and comprehensive TSV detection, spanning both  
215 traditional fusion-gene detection and the much broader class of general TSVs. SQUID exhibits far higher  
216 precision at similar sensitivities compared with WGS-based SV detection methods and pipelines of de novo  
217 transcriptome assembly and transcript-to-genome alignment. In addition, it has the ability to detect non-  
218 fusion-gene TSVs. These features are derived from its unique approach to predicting TSVs, whereby it  
219 constructs a consistent model of the underlying rearranged genome that explains as much of the data as pos-  
220 sible. In particular, it simultaneously considers both concordant and discordant reads, and by rearranging  
221 genome segments to maximize the number of concordant reads, SQUID generates a set of compatible TSVs

Figure 5: Tumor suppressor genes are affected by both fusion-gene and non-fusion-gene TSVs and generate transcripts with various features. (A) *ZFH3* is fused with a intergenic region after exon 3. The transcript stops at the inserted region, losing the rest of exons. (B) *ZFH3* is fused with a part of *MYLK3* anti-sense strand after exon 3. Codon and splicing signals are not preserved on anti-sense strand, thus *MYLK3* anti-sense insertion acts the same as intergenic region insertion, and causes transcription stop before reaching the rest of *ZFH3* exons. (C) *ASXL1* is fused with an intergenic region in the middle of exon 12. The resulting transcript contains a truncated *ASXL1* exon 12 and intergenic sequence. (D) The first 3 exons of *ASXL1* gene are joined with last 3 exons of *PDRG1*, resulting in a fused transcript containing 6 complete exons from both *ASXL1* and *PDRG1*.



222 that are most reliable in terms of the numbers of reads supporting them. Instead of a universal read support  
223 threshold, the objective function in SQUID naturally balances reads supporting and not supporting a candi-  
224 date TSV. This design is efficient in filtering out sequencing and alignment noise in RNA-seq, especially in  
225 the annotation-free context for predicting non-fusion-gene TSV events.

226 We use SQUID to analyze TCGA RNA-seq data of tumor samples. We identify BRCA to have a flatter  
227 distribution of number of per-sample TSVs than the other cancer types studied. We observe that non-fusion-  
228 gene TSVs are more likely to have intra-chromosomal TSVs than fusion-gene TSVs. This is likely due to  
229 the different sequence composition features in gene vs. non-gene regions. PRAD also stands out because  
230 the percentage of inter-chromosomal TSVs is the largest. Overall, these findings continue to suggest that  
231 different cancer types have different preferred patterns of TSVs, although the question remains whether  
232 these differences will hold up as more samples are analyzed and whether the different patterns are causal,  
233 correlated, or mostly due to non-functional randomness.

234 We also use SQUID to observe both non-fusion-gene and fusion-gene TSVs involving known tumor sup-  
235 pressor genes *ZFH3* and *ASXL1*. In these cases, transcription usually stops within the inserted region of  
236 the non-fusion-gene TSVs, which causes the TSG transcript to lose some of its exons, reasonably leading to  
237 downstream loss of function.

238 Other important uses and implications for general TSVs have yet to be explored and represent possible  
239 directions for future work. TSVs will impact accuracy of transcriptome assembly and expression quantifi-  
240 cation, and methodological advancements are needed to correct those downstream analyses for the effect  
241 of TSVs. For example, current reference-based transcriptome assemblers are not able to assemble from  
242 different chromosomes to handle the case of inter-chromosomal TSVs. In addition, expression levels of  
243 TSV-affected transcripts cannot be quantified if they are not present in the transcript database. Incorporat-  
244 ing TSVs into transcriptome assembly and expression quantification can potentially improve their accuracy.  
245 SQUID's ability to provide a new genome sequence that is as consistent as possible with the observed reads  
246 will facilitate its use as a pre-processing step for transcriptome assembly and expression quantification,  
247 though optimizing this pipeline remains a task for future work.

248 Several natural directions exist for extending SQUID. First, SQUID is not able to predict small deletions,  
249 instead, it treats the small deletions the same as intron-splitting events. This is to some extent a limitation of

250 using RNA-seq data: introns and deletions are difficult to distinguish, as both result in concordant split reads  
251 or stretched mate pairs. The use of gene annotations can somewhat address this problem. Second, when  
252 the RNA-seq reads are derived from a highly heterogeneous sample, SQUID is likely not able to predict  
253 all TSVs occurring in the same region if they are conflicting since it seeks a single, consistent genome  
254 model. Instead, SQUID will only pick the dominating one that is compatible with other predicted TSVs.  
255 One approach to handle this would be to iteratively re-run SQUID, removing reads that are explained at each  
256 step. Again, this represents an attractive avenue for future work.

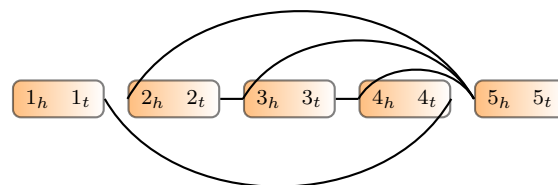
257 SQUID is open source and available at <http://www.github.com/Kingsford-Group/squid> and the scripts to  
258 replicate the computational experiments described here are available at <http://www.github.com/Kingsford-Group/squidtest>.

## 260 4 Methods

### 261 4.1 The computational problem: rearrangement of genome segments

262 We formulate the TSV detection problem as the optimization problem of rearranging genome segments to  
263 maximize the number of observed reads that are consistent (termed *concordant*) with the rearranged genome.  
264 This approach requires defining the genome segments that can be independently rearranged. It also requires  
265 defining what reads are consistent with a particular arrangement of the segments. We will encode both of  
266 these (segments and read consistency) within a *Genome Segment Graph* (GSG). See Figure 6 as an example.

Figure 6: Example of genome segment graph. Boxes are genome segments, each of which has two ends subscripted by  $h$  and  $t$ . The color gradient indicates the orientation from head to tail. Edges connect ends of genome segments.



267 **Definition 1** (Segment). A segment is a pair  $s = (s_h, s_t)$ , where  $s$  represents a continuous sequence in  
268 reference genome and  $s_h$  represents its head and  $s_t$  represents its tail in reference genome coordinates. In  
269 practice, segments will be derived from the read locations (Section 4.4).

270 **Definition 2** (Genome Segment Graph (GSG)). A genome segment graph  $G = (V, E, w)$  is an undirected  
271 weighted graph, where  $V$  contains both endpoints of each segment in a set of segments  $S$ , i.e.,  $V = \{s_h :$   
272  $s \in S\} \cup \{s_t : s \in S\}$ . Thus, each vertex in the GSG represents a location in the genome. An edge  
273  $(u, v) \in E$  indicates that there is evidence that the location  $u$  is in fact adjacent to location  $v$ . Weight  
274 function,  $w : E \rightarrow \mathbb{R}^+$ , represents the reliability of an edge. Generally speaking, the weight is the number  
275 of read alignments supporting the edge, but we allow a multiplier to calculate edge weight which will be  
276 discussed below. In practice,  $E$  and  $w$  will be derived from split-aligned and paired-end reads (Section 4.5).

277 Defining vertices by endpoints of segments is required to avoid ambiguity. Only knowing that segment  $i$  is  
278 connected with segment  $j$  is not enough to recover the sequence, since different relative positions of  $i$  and  
279  $j$  spell out different sequences. Instead, for example, an edge  $(i_t, j_h)$  indicates that the tail of segment  $i$  is  
280 connected head of segment  $j$ , and this specifies a unique desired local sequence with only another possibility  
281 of the reverse complement (i.e. it could be that the true sequence is  $i \cdot j$  or  $rev(j) \cdot rev(i)$ ; here  $\cdot$  indicates  
282 concatenation and  $rev(i)$  is the reverse complement of segment  $i$ ).

283 The GSG is similar to the breakpoint graph (Bafna and Pevzner 1996) but with critical differences. A  
284 breakpoint graph has edges representing both connections in reference genome and in target genome. While  
285 edges in the GSG only represents the target genome, and they can be either concordant or discordant. In  
286 addition, the GSG does not require that the degree of every vertex is two, and thus alternative splicing and  
287 erroneous edges can exist in the GSG.

288 Our goal is to reorder and reorient the segments in  $S$  so that as many edges in  $G$  are compatible with the  
289 rearranged genome as possible.

290 **Definition 3** (Permutation). A permutation  $\pi$  on a set of segments  $S$  projects a segment in  $S$  to a set of  
291 integers from 1 to  $|S|$  (the size of  $S$ ) representing the indices of the segments in an ordering of  $S$ . In other  
292 words, each permutation  $\pi$  defines a new order of segments in  $S$ .

293 **Definition 4** (Orientation Function). An orientation function  $f$  maps both ends of segments to 0 or 1:

$$f : \{s_h : s \in S\} \cup \{s_t : s \in S\} \rightarrow \{0, 1\}$$

294 subject to  $f(s_h) + f(s_t) = 1$  for all  $s = (s_h, s_t) \in S$ . An orientation function specifies the orientations of

295 all segments in  $S$ . Specifically,  $f(s_h) = 1$  means  $s_h$  goes first and  $s_t$  next, corresponding to forward strand  
296 of segment, and  $f(s_t) = 1$  corresponds to the reverse strand of the segment.

297 With a permutation  $\pi$  and an orientation function  $f$ , the exact and unique sequence of genome is determined.  
298 The reference genome also corresponds to a permutation and an orientation function, where the permutation  
299 is the identity permutation, and the orientation function maps all  $s_h$  to 1 and all  $s_t$  to 0.

300 **Definition 5** (Edge Compatibility). Given a set of segments  $S$ , a genome segment graph  $G = (V, E, w)$ , a  
301 permutation  $\pi$  on  $S$ , and an orientation function  $f$ , an edge  $e = (u_i, v_j) \in E$ , where  $u_i \in \{u_h, u_t\}$  and  
302  $v_j \in \{v_h, v_t\}$ , is compatible with permutation  $\pi$  and orientation  $f$  if and only if

$$1 - f(v_j) = \mathbf{I}[\pi(v) < \pi(u)] = f(u_i) \quad (1)$$

303 where  $\mathbf{I}[x]$  is the indicator function that is 1 if  $x$  is true and 0 otherwise. We write  $e \sim (\pi, f)$  if  $e$  is  
304 compatible with  $\pi$  and  $f$ .

305 The above two edge compatibility equations (1) require that, in order for an edge to be compatible with  
306 the rearranged and reoriented sequence determined by  $\pi$  and  $f$ , the edge needs to connect the right side  
307 of the segment in front to the left side of segment following it. As we will see in Section 4.5, edges of  
308 GSG are derived from reads alignments. An edge being compatible with  $\pi$  and  $f$  is essentially equivalent to  
309 the statement that the corresponding read alignments are concordant (Section 4.3) with respect to the target  
310 genome determined by  $\pi$  and  $f$ . When  $(\pi, f)$  is clear, we refer to edges that are compatible as concordant  
311 edges, and edges that are incompatible as discordant edges.

312 With the above definitions, we formulate an optimization problem as follows:

313 **Problem 1. Input:** A set of segments  $S$  and a GSG  $G = (V, E, w)$ .

314 **Output:** Permutation  $\pi$  on  $S$  and orientation function  $f$  that maximizes:

$$\max_{\pi, f} \sum_{e \in E} w(e) \cdot \mathbf{I}[e \sim (\pi, f)] \quad (2)$$

315 This objective function tries to find a rearrangement of genome segments  $(\pi, f)$ , such that when aligning  
316 reads to the rearranged sequence, as many reads as possible will be aligned concordantly. This objec-

317 tive function includes both concordant alignments and discordant alignments and sets them in competition,  
318 which will be effective in reducing false positives when tumor transcripts out-number normal transcripts.  
319 There is the possibility that some rearranged tumor transcripts are out-numbered by normal counterparts.  
320 In order to be able to detect TSV in this case, depending on the setting, we may weight discordant read  
321 alignments more than concordant read alignments. Specifically, for each discordant edge  $e$ , we multiply the  
322 weight  $w(e)$  by a constant  $\alpha$ , which represents our estimate of the ratio of normal transcripts over tumor  
323 counterparts.

324 The final TSVs are modeled as pairs of breakpoints. Denote the permutation and orientation corresponding  
325 to an optimally rearranged genome as  $(\pi^*, f^*)$  and those that correspond to reference genome as  $(\pi_0, f_0)$ .  
326 An edge  $e$  can be predicted as a TSV if  $e \sim (\pi^*, f^*)$  and  $e \not\sim (\pi_0, f_0)$ .

## 327 4.2 Integer linear programming formulation

328 We use integer linear programming (ILP) to compute an optimal solution  $(\pi^*, f^*)$  of Problem 1. To do this,  
329 we introduce the following boolean variables:

- 330 •  $x_e$ :  $x_e = 1$  if edge  $e \sim (\pi^*, f^*)$ , and  $x_e = 0$  if not.
- 331 •  $z_{uv}$ :  $z_{uv} = 1$  if segment  $u$  is before  $v$  in the permutation  $\pi^*$ , and 0 otherwise.
- 332 •  $y_u$ :  $y_u = 1$  if  $f^*(u_h) = 1$  for segment  $u$ .

333 With this representation, the objective function can be rewritten as

$$\max_{x_e, y_u, z_{uv}} w(e) \cdot x_e \quad (3)$$

334 We add constraints to the ILP derived from edge compatibility equations (1). Without loss of generality,  
335 we first suppose segment  $u$  is in front of  $v$  in the reference genome, and edge  $e$  connects  $u_t$  and  $v_h$  (which  
336 is a tail-head connection). Plugging in  $u_t$ , the first equation in (1) is equivalent to  $1 - \mathbf{1}[\pi(u) > \pi(v)] =$   
337  $1 - f(u_t)$ , and can be rewritten as  $\mathbf{1}[\pi(u) < \pi(v)] = f(u_h) = y_u$ . Note that  $\mathbf{1}[\pi(u) < \pi(v)]$  has the  
338 same meaning as  $z_{uv}$ ; it leads to the constraint  $z_{uv} = y_u$ . Similarly, the second equation in (1) indicates  
339  $z_{uv} = y_v$ . Therefore,  $x_e$  can only reach 1 when  $y_u = y_v = z_{uv}$ . This is equivalent to the inequalities (4)

340 below. Analogously, we can write constraints for other three types of edge connections: tail-tail connec-  
 341 tions impose inequalities (5); head-head connections impose inequalities (6); head-tail connections impose  
 342 inequalities (7):

$$\begin{aligned}
 x_e &\leq y_u - y_v + 1 & x_e &\leq y_u - (1 - y_v) + 1 \\
 x_e &\leq y_v - y_u + 1 & x_e &\leq (1 - y_v) - y_u + 1 \\
 x_e &\leq y_u - z_{uv} + 1 & x_e &\leq y_u - z_{uv} + 1 \\
 x_e &\leq z_{uv} - y_u + 1 & x_e &\leq z_{uv} - y_u + 1
 \end{aligned}
 \tag{4}$$

$$\begin{aligned}
 x_e &\leq (1 - y_u) - y_v + 1 & x_e &\leq (1 - y_u) - (1 - y_v) + 1 \\
 x_e &\leq y_v - (1 - y_u) + 1 & x_e &\leq (1 - y_v) - (1 - y_u) + 1 \\
 x_e &\leq (1 - y_u) - z_{uv} + 1 & x_e &\leq (1 - y_u) - z_{uv} + 1 \\
 x_e &\leq z_{uv} - (1 - y_u) + 1 & x_e &\leq z_{uv} - (1 - y_u) + 1
 \end{aligned}
 \tag{6}$$

$$\begin{aligned}
 x_e &\leq (1 - y_u) - (1 - y_v) + 1 \\
 x_e &\leq (1 - y_v) - (1 - y_u) + 1 \\
 x_e &\leq (1 - y_u) - z_{uv} + 1 \\
 x_e &\leq z_{uv} - (1 - y_u) + 1
 \end{aligned}
 \tag{7}$$

343 We also add constraints to enforce that  $z_{uv}$  forms a valid topological ordering. For each pair of nodes  $u$  and  
 344  $v$ , one must be in front of other, that is  $z_{uv} + z_{vu} = 1$ . In addition, for each triple of nodes,  $u$ ,  $v$  and  $w$ , they  
 345 cannot be all in front of another; one must be at the beginning of these three and one must be at the end.  
 346 Therefore we add  $1 \leq z_{uv} + z_{vw} + z_{wu} \leq 2$ .

347 Solving an ILP in theory takes exponential time, but in practice, solving the above ILP to rearrange genome  
 348 segments is very efficient. The key is that we can solve for each connected component separately. Because  
 349 the objective maximizes the sum of compatible edge weights, the best rearrangement of one connected com-  
 350 ponent is independent from the rearrangement of another because by definition there are no edges between  
 351 connected components.

### 352 4.3 Concordant and discordant alignments

353 Discordant alignments are alignments of reads that contradict library preparation in sequencing. Concordant  
 354 alignments are alignments of reads that agree with the library preparation. Take Illumina sequencing as an  
 355 example. In order for a paired-end read alignment to be concordant, one end should be aligned to the forward

356 strand and the other to the reverse strand, and the forward strand aligning position should be in front of the  
 357 reverse strand aligning position (Figure 7A). Concordant alignment traditionally used in WGS also requires  
 358 that a read cannot be split and aligned to different locations. But these requirements are invalid in RNA-seq  
 359 alignments because alignments of reads can be separated by an intron with unknown length.

360 We define concordance criteria separately for split-alignment and paired-end alignment. If one end of a  
 361 paired-end read is split into several parts and each part is aligned to a location, the end has split-alignments.  
 362 Denote the vector of the split alignments of an end to be  $R = [A_1, A_2, \dots, A_r]$  ( $r$  depends on the number  
 363 of splits). Each alignment  $R[i] = A_i$  is comprised of 4 components: chromosome (Chr), alignment starting  
 364 position (Spos), alignment ending position and orientation (Ori, with value either + or -). We require  
 365 that the alignments  $A_i$  are sorted by their position in read. A split-aligned end  $R = [A_1, A_2, \dots, A_r]$  is  
 366 concordant if all the following conditions hold:

$$\begin{aligned}
 A_i.Chr &= A_j.Chr && \forall i, \forall j \\
 A_i.Ori &= A_j.Ori && \forall i, \forall j \\
 A_i.Spos < A_j.Spos & \text{ if } A_i.Ori = + \text{ for all } i < j \\
 A_i.Spos > A_j.Spos & \text{ if } A_i.Ori = - \text{ for all } i < j
 \end{aligned} \tag{8}$$

367 If the end is not split, but continuous aligned, the alignment automatically satisfies equation (8). Denote the  
 368 alignments of  $R$ 's mate as  $M = [B_1, B_2, \dots, B_m]$ . An alignment of the paired-end read is concordant if  
 369 the following conditions all hold:

$$\begin{aligned}
 A_i.Chr &= B_j.Chr && \forall i, \forall j \\
 A_i.Ori &\neq B_j.Ori && \forall i, \forall j \\
 A_1.Spos < B_m.Spos & \text{ if } A_1.Ori = + \\
 A_m.Spos > B_1.Spos & \text{ if } A_1.Ori = -
 \end{aligned} \tag{9}$$

370 We only require the left-most split of the forward read  $R$  be in front of the left-most split of the reverse read  
 371  $M$  since the two ends in a read pair may overlap. In order for a paired-end read to be concordant, each  
 372 end should satisfy split-read alignment concordance (8), and the pair should satisfy paired-end alignment  
 373 concordance (9).

#### 374 **4.4 Splitting the genome into segments $S$**

375 We use a set of breakpoints to partition the genome. The set of breakpoints contains two types of positions:  
376 (1) the start position and end position of each interval of overlapping discordant alignments, (2) an arbitrary  
377 position in each 0-coverage region.

378 Ideally, both ends of a discordant read should be located in separate segments, otherwise, the discordant  
379 read contained in a single segment will always be discordant no matter how the segments are rearranged.  
380 Assuming discordant read alignments of each TSV pile up around the breakpoints and do not overlap with  
381 discordant alignments of other TSVs, we set a breakpoint on the start and end positions of each contiguous  
382 interval of overlapping discordant alignments.

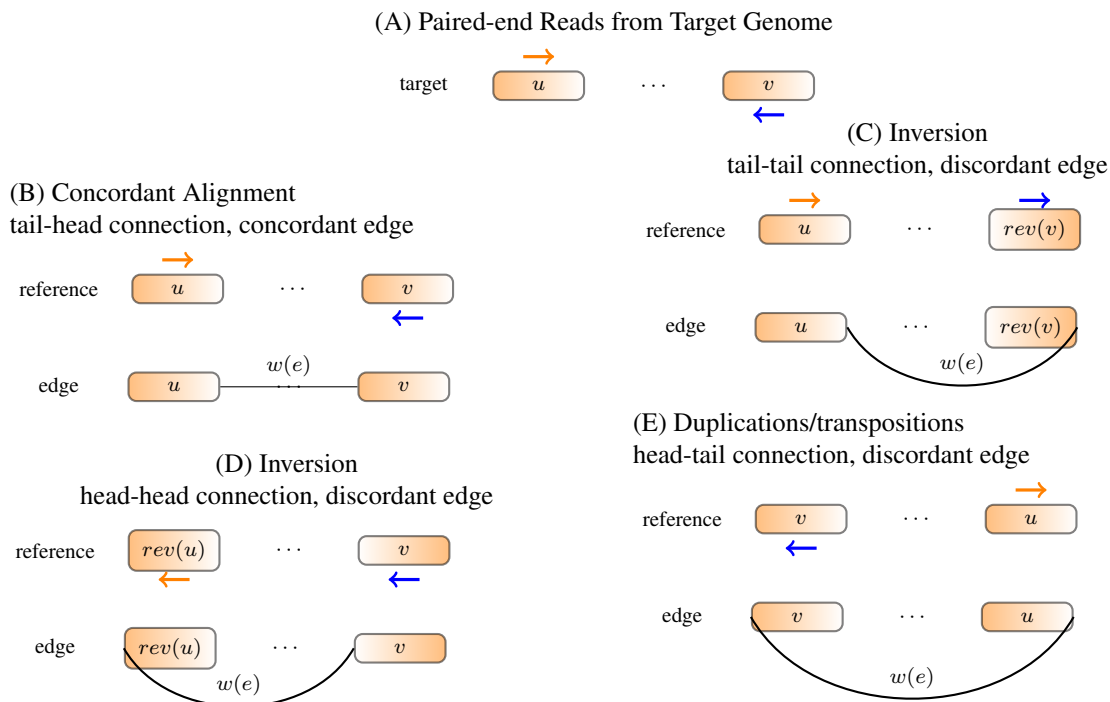
383 For each segment that contains discordant read alignments, it may also contain concordant alignments that  
384 connect the segment to its adjacent segments. To avoid having all segments in GSG connected to their  
385 adjacent segments and thus creating one big connected component, we pick the starting point of each 0-  
386 coverage region as a breakpoint. By adding those breakpoint, different genes will be in separate connected  
387 components unless some discordant reads support their connection. Overall, the size of each connected  
388 component is not very large: the number of nodes generated by each gene is approximately the number of  
389 exons located in them and these gene subgraphs are connected only when there is a potential TSV between  
390 them.

#### 391 **4.5 Defining edges in the genome segment graph**

392 In a GSG, an edge is added between two vertices when there are reads supporting the connection. For each  
393 read spanning different segments, we build an edge such that when traversing the segments along the edge,  
394 the read is concordant with the new sequence (equations (8) and (9)). Examples of deriving an edge from a  
395 read alignment are given in Figure 7. In this way, concordance of an alignment and compatibility of an edge  
396 with respect to a genome sequence is equivalent.

397 The weight of a concordant edge is the number of read alignments supporting the connection, while the  
398 weight of a discordant edge is the number of alignments supporting multiplied by discordant edge weight  
399 coefficient  $\alpha$ . Edges with very low read support are likely to be a result of alignment error, therefore we filter

Figure 7: Constructing edges from alignment. (A) Read positions and orientations generated from the target genome. (B) If the reference genome does not have rearrangements, the read should be concordantly aligned to reference genome. An edge is added to connect the right end of  $u$  to the left end of  $v$ . Traversing the two segments along the edge reads out  $u \cdot v$ , which is the same as reference. (C) Both ends of the read align to forward strand. An edge is added to connect the right end of  $u$  to the right end of  $rev(v)$ . Traversing the segments along the edge reads out sequence  $u \cdot rev(rev(v)) = u \cdot v$ , which recovers the target sequence and the read can be concordantly aligned to. (D) If both ends align to the reverse strand, an edge is added to connect the left end of front segment to the left end of back segment. (E) If two ends of a read point out of each other, an edge is added to connect the left end of front segment to the right end of back segment.



400 out edges with weight lower than a threshold  $\theta$ . Segments with too many connections to other regions are  
401 likely to have low mappability, so we also filter out segments connecting to more than  $\gamma$  other segments. The  
402 parameters  $\alpha$ ,  $\theta$ , and  $\gamma$  are the most important user-defined parameters to SQUID (Supplementary Table 1  
403 and Supplementary Figure S2).

#### 404 **4.6 Identifying TSV breakpoint locations**

405 Edges that are discordant in the reference genome indicate potential rearrangements in transcripts. Among  
406 those edges, some are compatible with the permutation and orientation from ILP. These edges are taken to be  
407 the predicted TSVs. For each edge that is discordant initially but compatible with the optimal rearrangement  
408 found by the ILP, we examine the discordant read alignments to determine the exact breakpoint located  
409 within related segments. Specifically, for each end of a discordant alignment, if there are 2 other read  
410 alignments that start or end in the same position and support the same edge, then the end of the discordant  
411 alignment is predicted to be the exact TSV breakpoint. Otherwise, the boundary of the corresponding  
412 segment will be output as the exact TSV breakpoint.

#### 413 **4.7 Simulation methodology**

414 Simulations with randomly added structural variations and simulated RNA-seq reads were used to evaluate  
415 SQUID's performance in situations with a known correct answer. RSVsim (Bartenhagen and Dugas 2013)  
416 was used to simulate SV on the human genome (Ensembl 87 or hg38) (Yates et al. 2015). We use the 5  
417 longest chromosomes for simulation (chromosome 1 to chromosome 5). RSVsim introduces 5 different  
418 types of SVs: deletion, inversion, insertion, duplication, and inter-chromosomal translocation. To vary the  
419 complexity of the resulting inference problem, we simulated genomes with 200 SVs of each type, 500 SVs  
420 of each type, and 800 SVs of each type. We generated 4 replicates for each level of SV complexity (200,  
421 500, 800). For inter-chromosomal translocations, we only simulate 2 events because only 5 chromosomes  
422 were used.

423 In the simulated genome with SVs, the original gene annotations are not applicable, and we cannot simulate  
424 gene expression from the rearranged genome. Therefore, for testing purposes, we interchange the role of the  
425 reference (hg38) and rearranged genome, and use the new genome as the reference genome for alignment,  
426 and hg38 with the original annotated gene positions as the target genome for sequencing. Flux Simula-

427 tor (Griebel et al. 2012) was used to simulate RNA-seq reads from the hg38 genome using the Ensembl  
428 annotation version 87 (Aken et al. 2016).

429 After simulating SVs on genome, we need to transform SVs into a set of TSVs, because not all SVs affect  
430 transcriptome, and thus not all SVs can be detected by RNA-seq. To derive the list of TSVs, we compare  
431 the positions of simulated SVs with the gene annotation. If a gene is affected by an SV, some adjacent  
432 nucleotides in the corresponding transcript may be located far part in the RSVsim-generated genome. The  
433 adjacent nucleotides can be consecutive nucleotides inside an exon if the breakpoint breaks the exon, or the  
434 end points of two adjacent exons if the breakpoint hits the intron. So for each SV that hits a gene, we find  
435 the pair of nucleotides that are adjacent in transcript and separated by the breakpoints, and convert them into  
436 coordinate of the RSVsim-generated genome, thus deriving the TSV.

437 Since there are no existing methods for annotation-free TSV detection, we compare SQUID to the pipeline  
438 of de novo transcriptome assembly and transcript-to-genome alignment. We also use the same set of sim-  
439 ulations to test whether existing WGS-based SV detection methods can be directly applied to RNA-seq  
440 data. For the de novo transcriptome assembly and transcript-to-genome alignment pipeline, we use all com-  
441 binations of the existing software Trinity (Grabherr et al. 2011), Trans-ABYSS (Robertson et al. 2010),  
442 GMAP (Wu and Watanabe 2005) and MUMmer3 (Kurtz et al. 2004). For WGS-based SV detection meth-  
443 ods, we test LUMPY (Layer et al. 2014) and DELLY2 (Rausch et al. 2012). We test both STAR (Dobin  
444 et al. 2013) and SpeedSeq (Chiang et al. 2015) (which is based on BWA-MEM (Li and Durbin 2009)) to  
445 align RNA-seq reads to the genome. LUMPY is only compatible with SpeedSeq output, so we do not test it  
446 with STAR alignments.

447 **Acknowledgements.** We thank Jacob West-Roberts for useful discussions. This research is funded in part  
448 by the Gordon and Betty Moore Foundation's Data-Driven Discovery Initiative through Grant GBMF4554  
449 to C.K., by the US National Science Foundation (CCF-1256087, CCF-1319998) and by the US National  
450 Institutes of Health (R21HG006913, R01HG007104), and by the Curci Foundation. C.K. received support  
451 as an Alfred P. Sloan Research Fellow. This project is funded, in part, under a grant (#4100070287) with the  
452 Pennsylvania Department of Health. The Department specifically disclaims responsibility for any analyses,  
453 interpretations or conclusions.

## References

- 454
- 455 Bronwen L Aken, Sarah Ayling, Daniel Barrell, Laura Clarke, Valery Curwen, Susan Fairley, Julio Fernan-  
456 dez Banet, Konstantinos Billis, Carlos García Girón, Thibaut Hourlier, et al. The Ensembl gene annotation  
457 system. *Database*, 2016, 2016.
- 458 Vineet Bafna and Pavel A Pevzner. Genome rearrangements and sorting by reversals. *SIAM Journal on*  
459 *Computing*, 25(2):272–289, 1996.
- 460 Christoph Bartenhagen and Martin Dugas. RSVSim: an R/Bioconductor package for the simulation of  
461 structural variations. *Bioinformatics*, 29(13):1679–1681, 2013.
- 462 Graham R Bignell, Thomas Santarius, Jessica CM Pole, Adam P Butler, Janet Perry, Erin Pleasance, Chris  
463 Greenman, Andrew Menzies, Sheila Taylor, Sarah Edkins, et al. Architectures of somatic genomic rear-  
464 rangement in human cancer amplicons at sequence-level resolution. *Genome Research*, 17(9):1296–1303,  
465 2007.
- 466 Ken Chen, John W Wallis, Michael D McLellan, David E Larson, Joelle M Kalicki, Craig S Pohl, Sean D  
467 McGrath, Michael C Wendl, Qunyuan Zhang, Devin P Locke, et al. BreakDancer: an algorithm for  
468 high-resolution mapping of genomic structural variation. *Nature Methods*, 6(9):677–681, 2009.
- 469 Colby Chiang, Ryan M Layer, Gregory G Faust, Michael R Lindberg, David B Rose, Erik P Garrison,  
470 Gabor T Marth, Aaron R Quinlan, and Ira M Hall. SpeedSeq: ultra-fast personal genome analysis and  
471 interpretation. *Nature Methods*, 12(10):966, 2015.
- 472 Nadia M Davidson, Ian J Majewski, and Alicia Oshlack. JAFFA: High sensitivity transcriptome-focused  
473 fusion gene detection. *Genome Medicine*, 7(1):43, 2015.
- 474 Michael WN Deininger, John M Goldman, and Junia V Melo. The molecular biology of chronic myeloid  
475 leukemia. *Blood*, 96(10):3343–3356, 2000.
- 476 Alexander Dobin, Carrie A Davis, Felix Schlesinger, Jorg Drenkow, Chris Zaleski, Sonali Jha, Philippe  
477 Batut, Mark Chaisson, and Thomas R Gingeras. STAR: ultrafast universal RNA-seq aligner. *Bioinform-*  
478 *atics*, 29(1):15–21, 2013.
- 479 Pedro AF Galante, Raphael B Parmigiani, Qi Zhao, Otávia L Caballero, Jorge E De Souza, Fábio CP

- 480 Navarro, Alexandra L Gerber, Marisa F Nicolás, Anna Christina M Salim, Ana Paula M Silva, et al.  
481 Distinct patterns of somatic alterations in a lymphoblastoid and a tumor genome derived from the same  
482 individual. *Nucleic Acids Research*, 39(14):6056–6068, 2011.
- 483 Manfred G Grabherr, Brian J Haas, Moran Yassour, Joshua Z Levin, Dawn A Thompson, Ido Amit, Xian  
484 Adiconis, Lin Fan, Raktima Raychowdhury, Qiandong Zeng, et al. Trinity: reconstructing a full-length  
485 transcriptome without a genome from RNA-Seq data. *Nature Biotechnology*, 29(7):644, 2011.
- 486 Thasso Griebel, Benedikt Zacher, Paolo Ribeca, Emanuele Raineri, Vincent Lacroix, Roderic Guigó, and  
487 Michael Sammeth. Modelling and simulating generic RNA-Seq experiments with the flux simulator.  
488 *Nucleic Acids Research*, 40(20):10073–10083, 2012.
- 489 Monica Hollstein, David Sidransky, Bert Vogelstein, and Curtis C Harris. p53 mutations in human cancers.  
490 *Science*, 253(5015):49–54, 1991.
- 491 Fereydoun Hormozdiari, Iman Hajirasouliha, Phuong Dao, Faraz Hach, Deniz Yorukoglu, Can Alkan,  
492 Evan E Eichler, and S Cenk Sahinalp. Next-generation VariationHunter: combinatorial algorithms for  
493 transposon insertion discovery. *Bioinformatics*, 26(12):i350–i357, 2010.
- 494 Matthew K Iyer, Arul M Chinnaiyan, and Christopher A Maher. ChimeraScan: a tool for identifying  
495 chimeric transcription in sequencing data. *Bioinformatics*, 27(20):2903–2904, 2011.
- 496 Stefan Kurtz, Adam Phillippy, Arthur L Delcher, Michael Smoot, Martin Shumway, Corina Antonescu, and  
497 Steven L Salzberg. Versatile and open software for comparing large genomes. *Genome Biology*, 5(2):  
498 R12, 2004.
- 499 Ryan M Layer, Colby Chiang, Aaron R Quinlan, and Ira M Hall. LUMPY: a probabilistic framework for  
500 structural variant discovery. *Genome Biology*, 15(6):1, 2014.
- 501 Heng Li and Richard Durbin. Fast and accurate short read alignment with Burrows–Wheeler transform.  
502 *Bioinformatics*, 25(14):1754–1760, 2009.
- 503 Donna Maglott, Jim Ostell, Kim D Pruitt, and Tatiana Tatusova. Entrez Gene: gene-centered information at  
504 NCBI. *Nucleic Acids Research*, 39(suppl 1):D52–D57, 2011.
- 505 Andrew McPherson, Fereydoun Hormozdiari, Abdalnasser Zayed, Ryan Giuliany, Gavin Ha, Mark GF Sun,

- 506 Malachi Griffith, Alireza Heravi Moussavi, Janine Senz, Nataliya Melnyk, et al. deFuse: an algorithm for  
507 gene fusion discovery in tumor RNA-Seq data. *PLoS Comput. Biol.*, 7(5):e1001138, 2011.
- 508 Fredrik Mertens, Bertil Johansson, Thoas Fioretos, and Felix Mitelman. The emerging complexity of gene  
509 fusions in cancer. *Nature Reviews Cancer*, 15(6):371–381, 2015.
- 510 Cancer Genome Atlas Network et al. Comprehensive molecular portraits of human breast tumors. *Nature*,  
511 490(7418):61, 2012.
- 512 Cancer Genome Atlas Research Network et al. Comprehensive molecular characterization of urothelial  
513 bladder carcinoma. *Nature*, 507(7492):315–322, 2014a.
- 514 Cancer Genome Atlas Research Network et al. Comprehensive molecular profiling of lung adenocarcinoma.  
515 *Nature*, 511(7511):543–550, 2014b.
- 516 Cancer Genome Atlas Research Network et al. The molecular taxonomy of primary prostate cancer. *Cell*,  
517 163(4):1011–1025, 2015.
- 518 Daniel Nicorici, Mihaela Satalan, Henrik Edgren, Sara Kangaspeska, Astrid Murumagi, Olli Kallioniemi,  
519 Sami Virtanen, and Olavi Kilkku. FusionCatcher - a tool for finding somatic fusion genes in paired-end  
520 RNA-sequencing data. *bioRxiv*, 2014. doi: 10.1101/011650.
- 521 Aaron R Quinlan, Royden A Clark, Svetlana Sokolova, Mitchell L Leibowitz, Yujun Zhang, Matthew E  
522 Hurles, Joshua C Mell, and Ira M Hall. Genome-wide mapping and assembly of structural variant break-  
523 points in the mouse genome. *Genome Research*, 20(5):623–635, 2010.
- 524 Tobias Rausch, Thomas Zichner, Andreas Schlattl, Adrian M Stütz, Vladimir Benes, and Jan O Korbel.  
525 DELLY: structural variant discovery by integrated paired-end and split-read analysis. *Bioinformatics*, 28  
526 (18):i333–i339, 2012.
- 527 Gordon Robertson, Jacqueline Schein, Readman Chiu, Richard Corbett, Matthew Field, Shaun D Jackman,  
528 Karen Mungall, Sam Lee, Hisanaga Mark Okada, Jenny Q Qian, et al. De novo assembly and analysis of  
529 RNA-seq data. *Nature Methods*, 7(11):909–912, 2010.
- 530 Dan R Robinson, Shanker Kalyana-Sundaram, Yi-Mi Wu, Sunita Shankar, Xuhong Cao, Bushra Ateeq,  
531 Irfan A Asangani, Matthew Iyer, Christopher A Maher, Catherine S Grasso, et al. Functionally recurrent

- 532 rearrangements of the MAST kinase and Notch gene families in breast cancer. *Nature Medicine*, 17(12):  
533 1646–1651, 2011.
- 534 Andrea Sboner, Xinmeng Jasmine Mu, Dov Greenbaum, Raymond K Auerbach, and Mark B Gerstein. The  
535 real cost of sequencing: higher than you think! *Genome Biology*, 12(8):125, 2011.
- 536 Charles J Sherr. Principles of tumor suppression. *Cell*, 116(2):235–246, 2004.
- 537 Philip J Stephens, David J McBride, Meng-Lay Lin, Ignacio Varela, Erin D Pleasance, Jared T Simpson,  
538 Lucy A Stebbings, Catherine Leroy, Sarah Edkins, Laura J Mudie, et al. Complex landscapes of somatic  
539 rearrangement in human breast cancer genomes. *Nature*, 462(7276):1005–1010, 2009.
- 540 A Sveen, S Kilpinen, A Ruusulehto, RA Lothe, and RI Skotheim. Aberrant RNA splicing in cancer; expres-  
541 sion changes and driver mutations of splicing factor genes. *Oncogene*, 35(19):2413–2428, 2015.
- 542 Scott A Tomlins, Daniel R Rhodes, Sven Perner, Saravana M Dhanasekaran, Rohit Mehra, Xiao-Wei Sun,  
543 Sooryanarayana Varambally, Xuhong Cao, Joelle Tchinda, Rainer Kuefer, et al. Recurrent fusion of  
544 TMPRSS2 and ETS transcription factor genes in prostate cancer. *Science*, 310(5748):644–648, 2005.
- 545 Jianghua Wang, Yi Cai, Wendong Yu, Chengxi Ren, David M Spencer, and Michael Ittmann. Pleiotropic  
546 biological activities of alternatively spliced TMPRSS2/ERG fusion gene transcripts. *Cancer Research*,  
547 68(20):8516–8524, 2008.
- 548 Thomas D Wu and Colin K Watanabe. GMAP: a genomic mapping and alignment program for mRNA and  
549 EST sequences. *Bioinformatics*, 21(9):1859–1875, 2005.
- 550 Xudong Wu, Ida Holst Bekker-Jensen, Jesper Christensen, Kasper Dindler Rasmussen, Simone Sidoli, Yan  
551 Qi, Yu Kong, Xi Wang, Yajuan Cui, Zhijian Xiao, et al. Tumor suppressor ASXL1 is essential for  
552 the activation of *INK4B* expression in response to oncogene activity and anti-proliferative signals. *Cell*  
553 *Research*, 25(11):1205–1218, 2015.
- 554 Andrew Yates, Wasii Akanni, M Ridwan Amode, Daniel Barrell, Konstantinos Billis, Denise Carvalho-  
555 Silva, Carla Cummins, Peter Clapham, Stephen Fitzgerald, Laurent Gil, et al. Ensembl 2016. *Nucleic*  
556 *Acids Research*, 44(D1):D710–D716, 2015.
- 557 Jin Zhang, Nicole M White, Heather K Schmidt, Robert S Fulton, Chad Tomlinson, Wesley C Warren,

- 558 Richard K Wilson, and Christopher A Maher. INTEGRATE: gene fusion discovery using whole genome  
559 and transcriptome data. *Genome Research*, 26(1):108–118, 2016.
- 560 Qi Zhao, Otavia L Caballero, Samuel Levy, Brian J Stevenson, Christian Iseli, Sandro J De Souza, Pedro A  
561 Galante, Dana Busam, Margaret A Leversha, Kalyani Chadalavada, et al. Transcriptome-guided charac-  
562 terization of genomic rearrangements in a breast cancer cell line. *Proceedings of the National Academy  
563 of Sciences, USA*, 106(6):1886–1891, 2009.

## 564 **Supplementary Text**

565 All experiments here are performed with SQUID version 1.0.

### 566 **Using de novo assembly and transcript to genome alignment to predict TSV**

567 For the pipeline of de novo transcriptome assembly and transcript-to-genome alignment, the direct output is  
568 a series of alignment pieces for each assembled transcript. To derive TSV from the pieces of alignment of  
569 each transcript, we still need to use the split-read alignment concordance criteria (8) and the edge-building  
570 approach. In the case of no TSV, equation (8) still holds, since a transcript is generated from one strand of  
571 one chromosome, without rearrangements but only deletion of introns. Any violation of (8) is treated as a  
572 TSV. Here TSVs are still able to be represented by edges in GSG, where segments are the intervals of each  
573 piece of alignment, and edges are added in the same principle that traversing segments along the edges will  
574 result in a concordant alignment of the assembled transcript. The positions of both breakpoints in a TSV are  
575 exactly the two positions linked by the discordant edge, and the orientations corresponds to the connection  
576 type of the edge.

### 577 **Processing TCGA RNA-seq data**

578 We use STAR aligner to align TCGA RNA-seq reads to Ensemble genome 87 with the corresponding gene  
579 annotation. STAR aligner is set with the option of outputting chimeric alignments with hanging length 15bp.  
580 The chimeric alignments generated by STAR are further filtered out if the paired-end reads can be aligned  
581 concordantly by SpeedSeq aligner.

582 SQUID is applied to concordant alignment generated by STAR and filtered chimeric alignment. The dis-  
583 cordant edge weight coefficient  $\alpha$  is set to be 1, that is, we require tumor transcripts to dominate normal  
584 transcripts in order to predict corresponding TSVs.

585 A large number of fusions between immunoglobulin genes are predicted by SQUID. However, there is  
586 possibility that B cells are in the mixture of sequencing and have very high expression of immunoglobulin  
587 genes (Ig). We cannot tell whether Ig rearrangements are generated by tumor cells or B cells. Therefore, we  
588 exclude Ig TSVs during post-processing and exclude them from the descriptive statistics. Note that SQUID  
589 does not exclude Ig TSVs internally, because Ig expression and VDJ recombination have been observed to

590 exist in tumor cells, and revealing the role of Ig in tumor can deepen our understanding of cancer. When  
591 normal cells are removed from tumor samples, using SQUID to predict Ig TSV will help the study of Ig and  
592 tumor.

### 593 SQUID parameters

Table 1: Value of SQUID's parameters used in experiments

Symbol	Description	Value
$\gamma$	segment degree threshold	4
$\theta$	edge weight threshold	5
$\alpha$	discordant edge weight coefficient	8 (simulation and HCC cell line), 1 (TCGA)
$mq$	minimum mapping quality	255 (STAR), 1 (SpeedSeq)
$pq$	low Phred quality threshold	4 ( $p = 10^{-0.4}$ )
$l$	maximum allowed low Phred quality length	10

594 Note:  $mq$ ,  $pq$  and  $l$  are controls for sequencing quality and mapping quality. If mapping quality of a read is  
595 less than threshold  $mq$ , the read will not be used in edge building. If the read has a low sequencing, in terms  
596 of having more than  $l$  bases of sequencing quality lower than  $pq$ , the read will not be used in edge building.

597 **Supplementary Figures**

Figure S1: Number of samples with RNA-seq or WGS data in TCGA

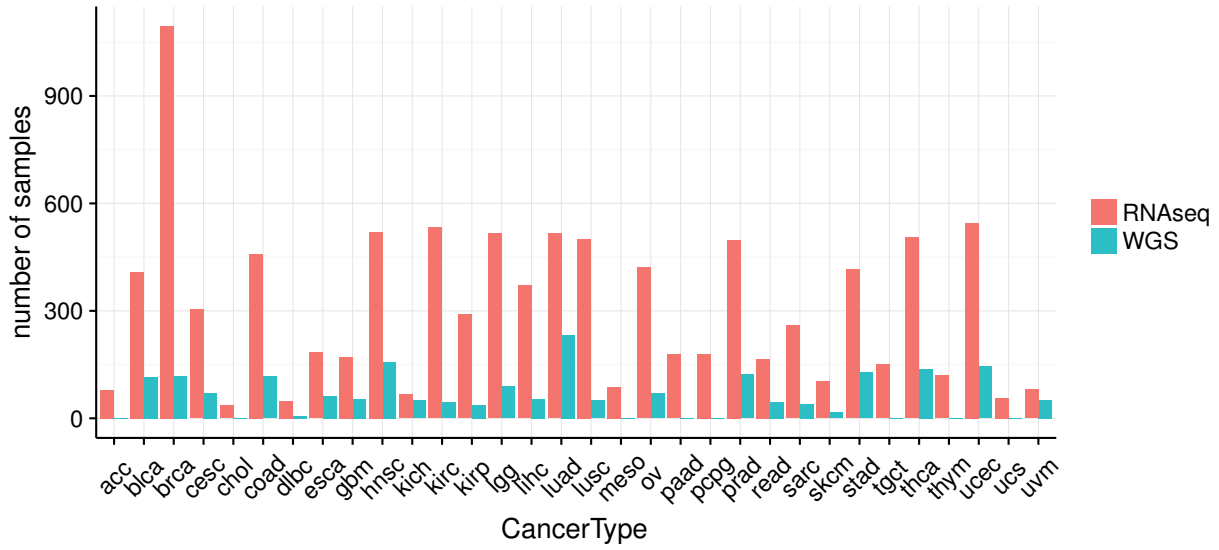


Figure S2: Specificity and sensitivity of SQUID against different value of discordant edge weight coefficient. (A) HCC1954 cell line. Sensitivity does not change when increasing discordant edge weight coefficient, indicating rearranged tumor transcripts out-number their normal counterparts. Specificity decreases slightly because SQUID predicts more as discordant edge weight coefficient increases. (B) HCC1395 cell line. Sensitivity and specificity reach the highest at discordant edge weight coefficient 8 and remain unchanged at 9 and 10. Some normal transcripts out-number the rearranged tumor transcripts, increasing this parameter allows SQUID to capture these TSVs.

